nature photonics

ARTICLES

PUBLISHED ONLINE: 27 JUNE 2016 | DOI: 10.1038/NPHOTON.2016.121

Two-photon direct laser writing of ultracompact multi-lens objectives

Timo Gissibl[1]*, Simon Thiele[2], Alois Herkommer[2] and Harald Giessen[1]

Current lens systems are restricted in size, shape and dimensions by limitations of manufacturing. Multi-lens elements with non-spherical shapes are required for high optical performance and to correct for aberrations when imaging at wide angles and large fields. Here we present a novel concept in optics that overcomes all of the aforementioned difficulties and opens the new field of 3D printed micro- and nano-optics with complex lens designs. We demonstrate the complete process chain, from optical design, manufacturing by femtosecond two-photon direct laser writing and testing to the application of multi-lens objectives with sizes around 100 μm, and validate their high performance and functionality by quantitative measurements of the modulation transfer function and aberrations. The unprecedented flexibility of our method paves the way towards printed optical miniature instruments such as endoscopes, fibre-imaging systems for cell biology, new illumination systems, miniature optical fibre traps, integrated quantum emitters and detectors, and miniature drones and robots with autonomous vision.

Additive manufacturing enables new and unprecedented engineering and production possibilities that are predicted to have an enormous impact in the twenty-first century. The technology allows for the simple three-dimensional (3D) printing of volumetric objects directly from a computer-aided design[1]. So far, additively manufactured objects are mostly fabricated from metals, ceramics and opaque plastics. There are a number of different fabrication methods to manufacture small and high-performance micro-optical systems[2–10]; however, these technologies suffer from drawbacks such as limited miniaturization, inability to combine multiple elements, restrictions in designing the surfaces[2–4,11] and problems with the alignment[12].

Multiphoton lithography is one of various 3D printing technologies that realize the fabrication of 3D objects[13–15]. Using femtosecond laser pulses and two-photon absorption, this manufacturing method takes 3D printing down to submicrometre feature sizes and therefore pushes the ongoing trend of miniaturization forwards. Direct laser writing with highly transparent photoresists enables 3D printing to enter the realm of manufacturing optical elements at the micro- and nanometre scale[16–22]. Thus the precise fabrication of complex optical elements on demand becomes possible.

We demonstrate that 3D direct laser writing is a suitable tool for fabricating complex multi-lens optical systems that show high optical performances and tremendous compactness. Until now multi-lens optics that have comparable performances are considerably larger[12,23] and at the same time do not show the manifold compound structures and possibilities presented here. Our optical devices consist of several different free-form lens elements with air in between. This work is right at the interface between micro- and nano-optics and represents a paradigm shift for micro-optics. It takes only a few hours from lens design through production and testing to the final working optical device.

Endoscopic applications will allow for non-invasive and non-destructive examination of small objects in the medical as well as the industrial sector and serve as a hallmark application of this new technology. Figure 1 depicts an optical fibre equipped with a 3D printed multi-lens system for imaging the interior of a hollow organ or a cavity inside the body. Using a very small injection cannula with an outer diameter of only 412 μm (27 gauge) together with the fibre-coupled printed compound microscope objective lens, the insertion can be easily accomplished.

In this Article we demonstrate the capabilities of 3D dip-in laser lithography to manufacture high-quality optical compound lenses with outstanding performances[24]. We realize a variety of optical elements with different features for numerous applications. The optical performance is quantified and analysed by measuring the optical modulation transfer function (MTF) and the longitudinal (axial) chromatic aberration. We also characterize the roughness of the surfaces by atomic force microscope measurements. As

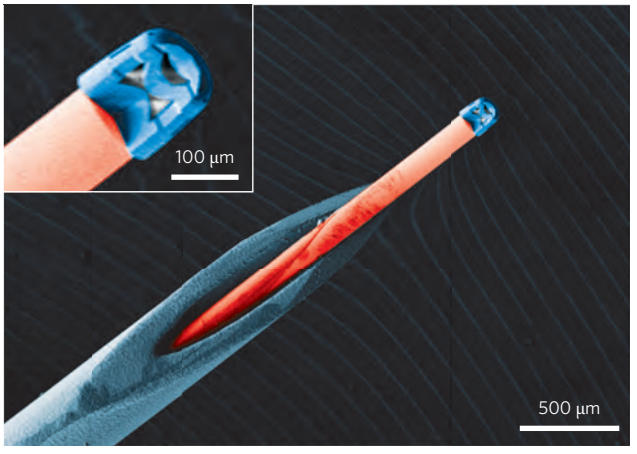

Figure 1 | Coloured SEM image of a triplet lens objective attached to an optical fibre inserted into the hollow needle of a syringe. The compound objective lens (blue) consists of five refractive surfaces for imaging applications and is directly fabricated on the optical fibre (red). The fibre is emerging from a hollow needle (27 gauge, outer diameter 412 μm, inner diameter 210 μm) to demonstrate the possibility of endoscopic applications. The objective lens is fabricated in a cutout fashion for better visibility. The inset shows a magnified image of the fibre tip with the objective.

[1]4th Physics Institute and Research Center SCoPE, University of Stuttgart, Pfaffenwaldring 57, 70569 Stuttgart, Germany. [2]Institute for Applied Optics (ITO) and Research Center SCoPE, University of Stuttgart, Pfaffenwaldring 9, 70569 Stuttgart, Germany. *e-mail: t.gissibl@pi4.uni-stuttgart.de

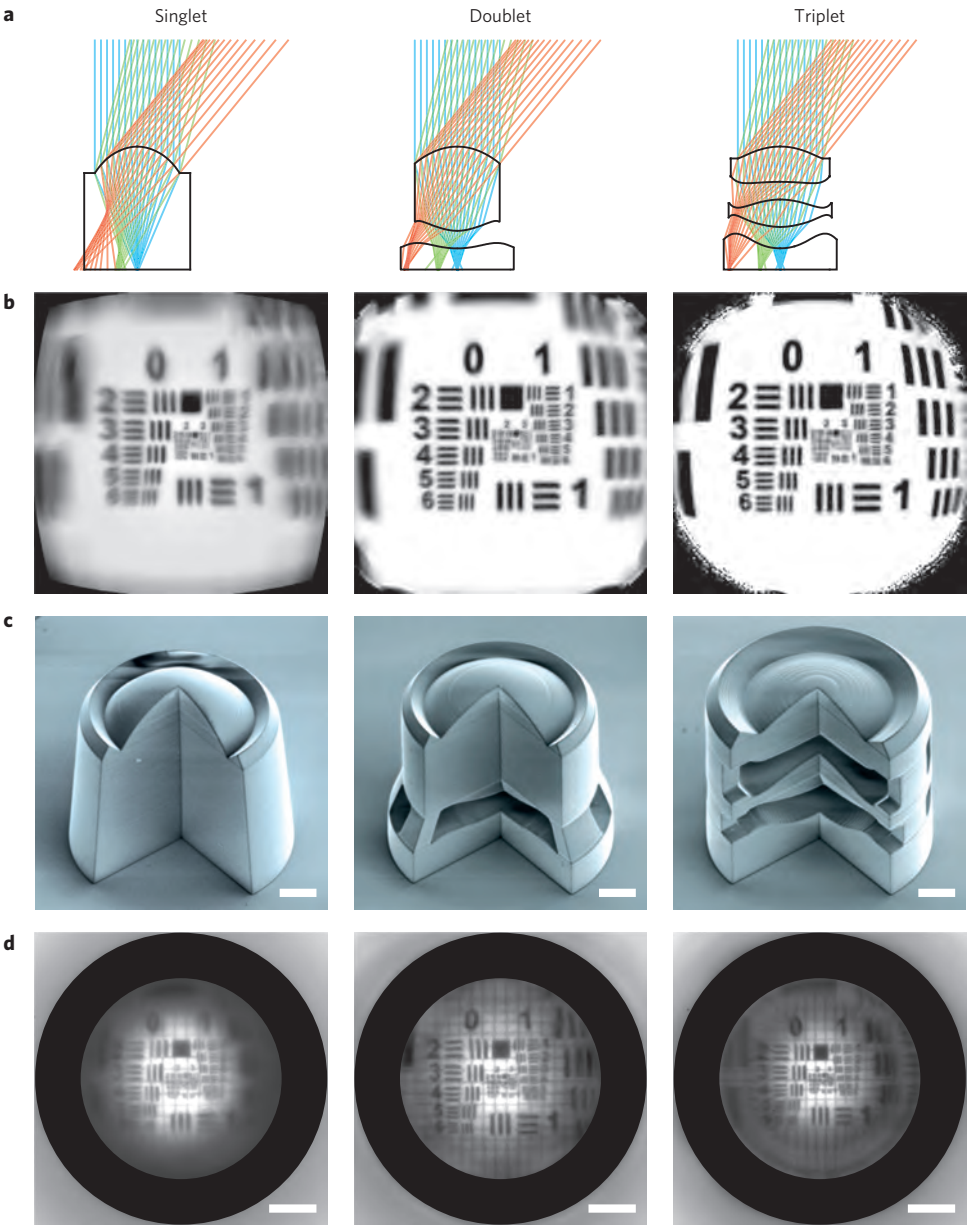

Figure 2 | Comparison of singlet, doublet and triplet printed lens systems. Each compound objective has a total height of around 115 μm and is fabricated on a 170-μm-thick glass substrate by 3D femtosecond direct laser writing. The focal length is 68.3 μm at a wavelength of 550 nm. **a**, Optical design of singlet, doublet and triplet lenses as optimized in ZEMAX. **b**, Simulated image of the USAF 1951 resolution test chart. **c**, Scanning electron microscope images of the singlet, doublet and triplet lenses printed with a 90° piece cut out to provide a better view of the different lenses. **d**, Recorded USAF 1951 resolution test chart imaged by the various printed lenses. Images taken with a Nikon microscope equipped with a 50× objective (NA 0.55) and CCD camera (2,448 × 2,050 pixel^2). The distance between the lens and target is 20 mm. The FOV is 80°. Scale bars, 20 μm.

examples for applications, we show the performance of multi-lens systems manufactured on optical imaging fibres with 1,600 pixels as well as on CMOS image sensors with pixel sizes of 1.4 × 1.4 μm^2, whereas our lenses have diameters of not more than 120 μm and heights between 100 and 200 μm.

Design and fabrication

The submicrometre compound elements presented in this Article are designed and optimized within the optical design software ZEMAX. Aspheric surfaces are used to compensate for optical aberrations and improve the image quality for each surface. The lens design is exported and converted into a stereolithographic file format. Subsequently, the compound lenses are fabricated by 3D dip-in direct laser writing using a commercially available femtosecond laser lithography system (Photonic Professional GT, Nanoscribe GmbH, Germany)[24]. The complete optical compound system is manufactured from one single material. We therefore use a photoresist that exhibits high optical quality (IP-S, Nanoscribe GmbH). Several different singlet lenses are combined into a compound lens in a supporting shell, which fulfils a variety of requirements at once. On the one hand, it axially and laterally aligns the individual optical elements and therefore prevents tilting; on the other hand, it serves as protection. The shell is equipped with several holes that are required for the development process but can also be used for the subsequent deposition of an antireflection coating by atomic layer deposition (ALD) on the surfaces. Further information concerning the design and fabrication is included in the Methods.

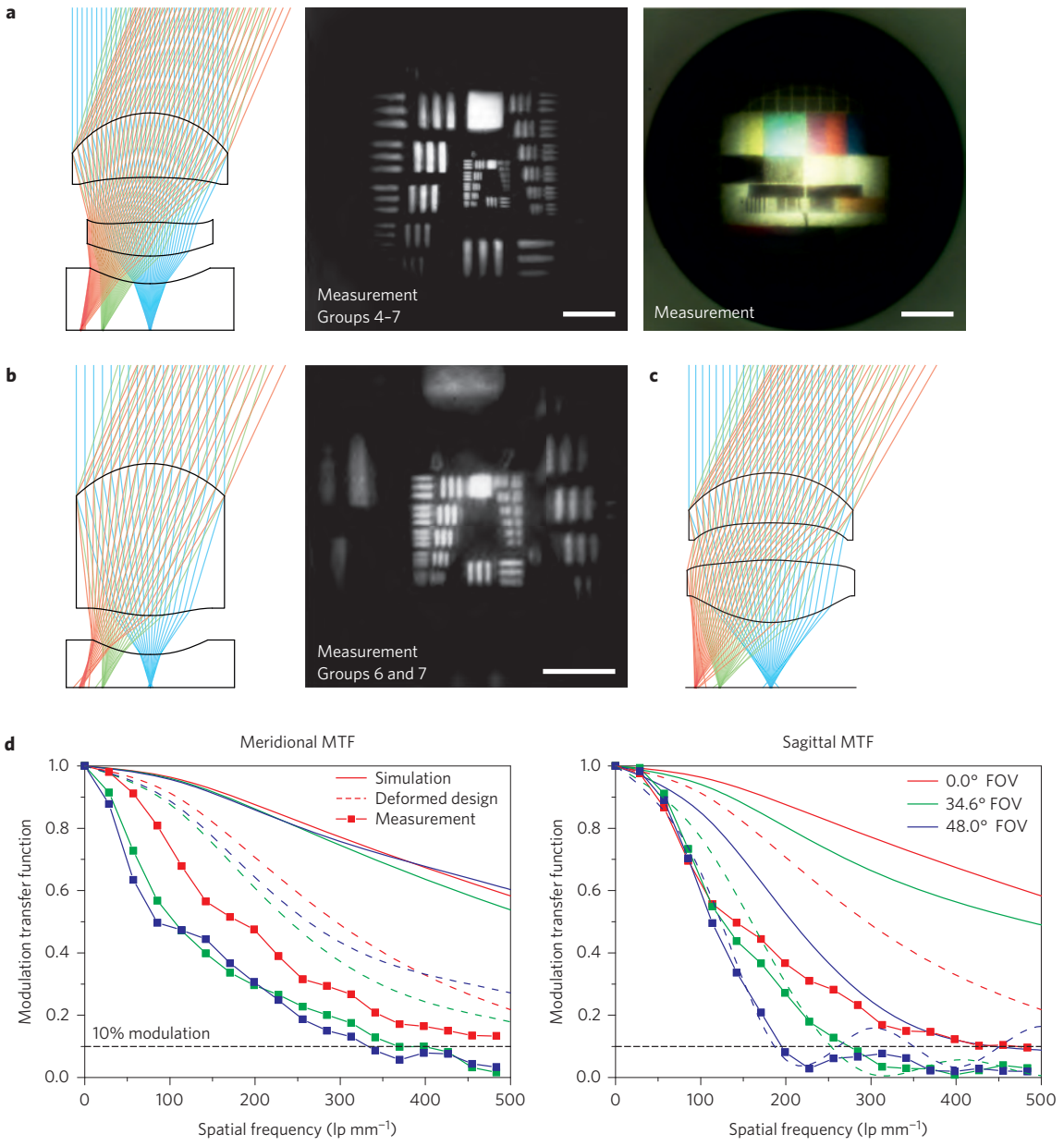

Figure 3 | Performance measurement using the USAF 1951 resolution test chart, the Telefunken FuBK test card and the knife-edge methodology to determine the MTF. a, Ray-tracing design of a triplet lens system optimized in ZEMAX (left), an image of the USAF 1951 resolution test chart (groups 4–7) taken through the triplet lens at a distance of 1 mm behind the lens (centre) and an image of the Telefunken FuBK test card at a distance of 20 mm (right). Scale bars, 20 μm. **b**, Ray-tracing design of a doublet lens system (left) and an image of the USAF 1951 resolution test chart at a distance of 1 mm behind the lens (right). The three bars in group 6, element 5, corresponding to 101.6 lp mm^{-1} are clearly visible. Scale bar, 10 μm. **c**, Ray-tracing design of a doublet lens system with four refractive surfaces optimized in ZEMAX. **d**, Simulation and measurement of the meridional and sagittal MTF for different angles and for the doublet lens of **c**. The appearance, particularly of the resolution charts, might vary when viewed in print or on the computer screen, depending on the brightness and contrast settings.

Measurements and discussion

As a first example of our ultracompact lens systems, we manufacture compound lenses with different numbers of surfaces starting from one to five refractive interfaces. Figure 2 depicts a comparison between singlet, doublet and triplet lens systems, fabricated on a 170 μm thick glass substrate. The lens systems are designed to have a large field of view (FOV) of 80°. As can be seen from the optical design and the ray-tracing simulations in Fig. 2a, the performance improves as the number of interfaces increases. Although in the singlet lens design the rays across the field are not well imaged onto one single point, in the triplet lens design the rays incident from different angles converge into a single point in the image plane at the rightmost interface. Simulations with a USAF 1951 resolution test chart in Fig. 2b confirm this observation. The simulation of the singlet lens exhibits strong field dependent aberrations that are recognizable from the blurry edges of the image. Additionally, the magnification of the singlet lens is non-uniform across the image field. This barrel distortion is clearly visible at the edges of the image in the singlet simulation of Fig. 2b. By increasing the number of refractive interfaces, the field dependent optical aberrations—namely field curvature, coma, astigmatism and distortion—can be compensated. Figure 2c shows scanning electron microscope (SEM) images of the singlet, doublet and triplet lenses that have been manufactured with a 90° slice cut out for demonstration purposes.

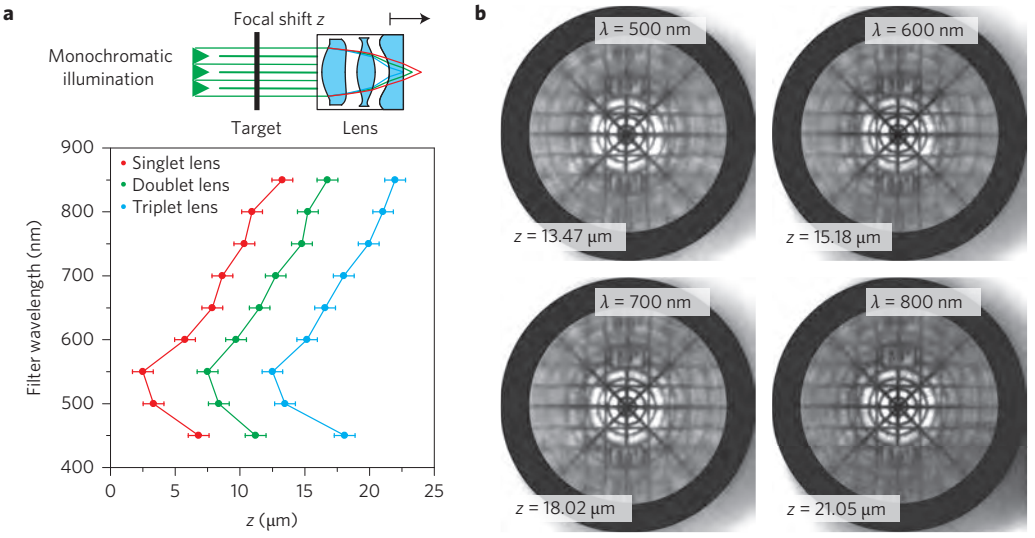

Figure 4 | Measurement of the longitudinal (axial) chromatic aberration. a, Relative focal shift due to the longitudinal chromatic aberration for the singlet, doublet and triplet lens systems introduced in Fig. 2 for different wavelengths. The curves are displaced horizontally by 5 μm relative to each other for better visibility. **b**, Images of a test chart taken with the triplet lens system and a CCD camera over a wavelength range of 500–800 nm. A white light lamp with 40 nm-wide bandpass filters is used for illumination. Each ring corresponds to a 10° FOV. The outer ring corresponds to an 80° FOV. High image contrasts up to 50° of the FOV are observed. The relative *z* position of each image is chosen to obtain highest contrast. The distance between the target and the lens is 5 mm.

Each lens element is manufactured layer-by-layer from the same material. The diameters of the lenses are 120 μm (including the supporting shell). The SEM image confirms the high manufacturing quality and the excellent shape fidelity. To quantify the fabrication tolerances the surface is also characterized by atomic force microscope measurements. A surface roughness of less than 15 nm (root mean squared; r.m.s.) is easily feasible (Supplementary Fig. 1) as we use a photoresist that exhibits high proximity effects. Figure 2d depicts the optical performance of the singlet, doublet and triplet lenses achieved by imaging the USAF 1951 resolution test chart at a distance of about 20 mm. We imaged the rightmost surface using an optical microscope with a 50× objective lens and a CCD camera. The true-colour images are subsequently converted to greyscale intensity images. The simulations and measurements of the imaging performance exhibit good agreement. Just as in the simulations, the barrel distortion and other field dependent aberrations disappear as the number of refractive surfaces is increased. In the measurements the natural illumination drop-off and the effect of optical vignetting are visible. The optical vignetting is caused by the physical dimensions of the optical system, whereas the natural drop is caused by cos law for the relative illumination[4]. The drop-off is particularly enhanced for the triplet lens system, as Fresnel reflections at five interfaces are substantial.

The quantitative optical performance of different doublet and triplet systems is further investigated by using different test charts. In Fig. 3a the imaging properties of a triplet lens system are analysed. The left image shows the optical ray-tracing design of the lens. The objective consists of five refractive interfaces that are all aspheric in shape. The FOV in the object space is designed to be 47°. The last surface is attached to a 170 μm thick substrate on which the lens is fabricated. Using the USAF 1951 resolution test chart we achieve a maximal resolution of 128 line pairs per mm (lp mm^{-1}, which corresponds to element 1 of group 7 of the test chart (centre image of Fig. 3a). The 3D printed optical system and the resolution chart are separated by a distance of around 1 mm. The colour fidelity is investigated by a Telefunken FuBK test card in the right image of Fig. 3a. The image exhibits a yellowish hue, which is caused by the remaining photoinitiator in the lens material. By adjusting the colour balance of the CMOS sensor the colour distortion can be eliminated.

In Fig. 3b the performance measurement for a doublet lens system with three refractive surfaces is depicted. On the left-hand side the optical design optimized in ZEMAX is shown. The lens is designed to have an FOV in the object space of 50° and an imaging area diameter of 100 μm. The measurement is displayed on the right. The optical performance is measured with a USAF 1951 resolution test chart at a distance of around 1 mm. A 100× objective lens is used to record the image. We achieve a resolving power of 101.6 lp mm^{-1}, associated with element 5 of group 6 and corresponding to a line width of 4.92 μm in the USAF 1951 resolution test chart. The images appear blurry due to chromatic aberrations.

In Fig. 3c a doublet lens system with four refractive interfaces is shown. The optical system has an FOV in the object space of 60° and exhibits a meridional and sagittal MTF of at least 195 lp mm^{-1} for a 10% modulation contrast over the complete FOV. The MTF is measured using a knife-edge method. To accomplish this, the sharp edge of a razor blade is imaged by the 3D printed compound lens and a 50× objective onto the CCD camera at various field positions and with different orientations. More measurement and evaluation details are provided in Supplementary Fig. 2 as well as in the Methods. For small angles, a resolving power of more than 400 lp mm^{-1} is achieved. Compared to wafer-level objective lenses[12,23] fabricated by micro imprint technology with edge lengths of 500 μm (ref. 25) our 3D printed compound lenses show better resolving powers and considerably higher fields of view of up to 60° in the object space.

Owing to a possible non-uniform shrinkage of the photoresist during the fabrication and development process, the final shape of the optical system is not perfectly as-designed, which might be the source of the deviation between the measurements and simulations (see Fig. 3d). Therefore, in a first approximation we additionally plot a simulation of the MTF (dashed lines in Fig. 3d), where the radius of curvature part of the aspheric surface shape is reduced by 8%. This corresponds to an axial deviation of roughly 2 μm in a radial distance of 50 μm for a radius of curvature of 80 μm. The simulation shows that the origin of the deviations can be partly explained by a shrinkage of the 3D printed lenses. The sagittal MTF shows better agreement between experiment and simulation than the meridional MTF. This suggests an anisotropic shrinking process, but the details and the dependence on the exposure and

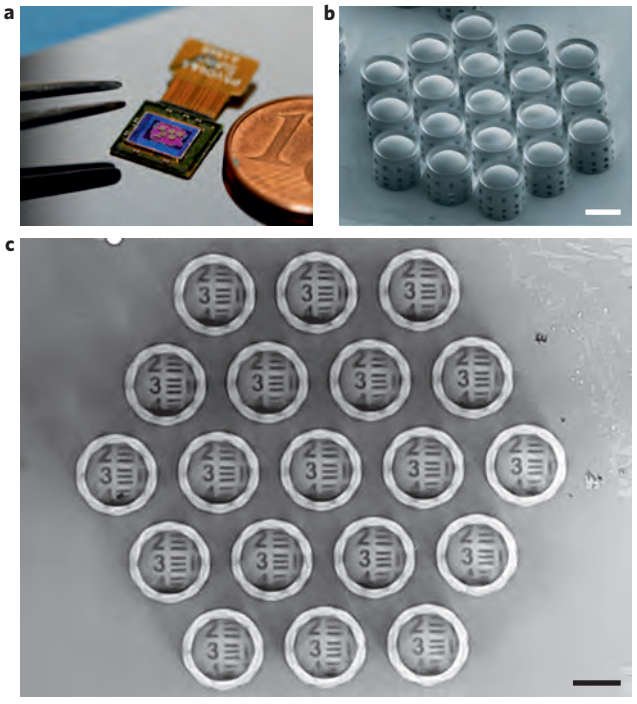

Figure 5 | Regular arrangement of doublet lens systems directly fabricated on a CMOS image sensor. a, Photograph of an Omnivision 5647 CMOS image sensor with doublet lenses. The CMOS-chip has a pixel size of $1.4 \times 1.4\ \mu m^2$. **b**, Scanning electron microscope image of the hexagonal lens arrangement. Each doublet lens system has a diameter of 120 μm and a height of 128 μm. Scale bar, 100 μm. **c,** Image of a part of the USAF 1951 resolution test chart at a distance of 30 mm taken through a hexagonal lens arrangement. The elements are of group −2. The image section consists of 640 × 480 pixels. Scale bar, 70 μm = 50 pixels.

writing condition will be investigated in the future. Furthermore, the uncertainties of some of the material properties as well as material inhomogeneities might lead to deviations between the results of experiments and simulations, which predict modulation depths of up to 0.5 at 500 lp mm^{-1}.

Chromatic aberrations are analysed for the singlet, doublet and triplet lenses introduced in Fig. 2. Bandpass filters with a width of 40 nm in the range from 450 to 850 nm are used for target illumination. By adjusting the focal position at each wavelength the image is sharpened and the highest contrast is achieved. Figure 4a shows the measurements of the longitudinal (axial) chromatic aberrations for the singlet, doublet and triplet lenses. For better visibility, the curves are displaced by 5 μm relative to each other. All three lenses show the same chromatic aberration behaviour. Owing to dispersion effects in the lens material at each wavelength, the target is imaged onto a different focal plane. To avoid this effect a classical achromatic lens design consisting of two materials with different Abbe numbers will be used in the future. In this case, the direct laser writing process will be accomplished by using different photosensitive materials in separate fabrication steps. Figure 4b depicts images of a test chart at different wavelengths from 500 to 800 nm at different focal positions. The test chart is imaged by the triplet lens introduced in Fig. 2. A high image contrast can be observed up to a 50° FOV. The test chart consists of concentric rings at an azimuthal angle separation of a 10° FOV. The outer ring corresponds to an 80° FOV in object space, which agrees very well with the optical design.

To make the capability of the system to integrate the production of 3D printed ultra-compact compound lenses evident, we demonstrate direct manufacturing on image sensors and imaging fibers.

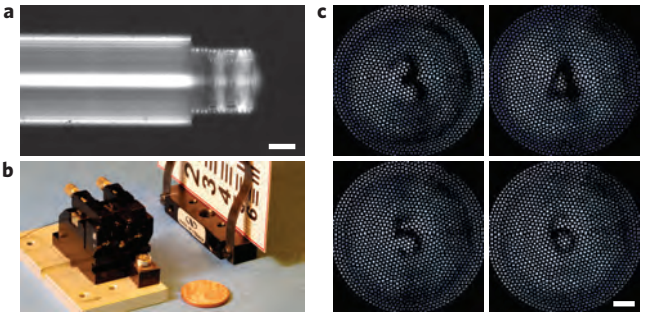

Figure 6 | Triplet objective lens system fabricated directly on an imaging fibre. The diameter of the imaging area is 145 μm, with 1,600 single mode cores of 4 μm diameter each. **a**, Microscope image of the side view of the triplet lens introduced in Fig. 2. Scale bar, 50 μm. **b**, Measurement set-up. **c**, Image of a part of the USAF 1951 resolution test chart through a 170-cm-long piece of an imaging fibre with 1,600 pixels. The numbers are the notations of the elements of group 0. The distance between the fibre end facet and the test chart is 3 mm. Scale bar, 20 μm.

Figure 5a depicts several arrays of doublet lens systems with four refractive interfaces directly fabricated on an Omnivision 5647 CMOS image sensor. The doublet lens with a 60° FOV and a designed f-number of 0.78 has already been introduced in Fig. 3c. The five megapixel CMOS image sensor possesses a total active area of $2{,}592 \times 1{,}944$ pixel². Each pixel has a size of $1.4 \times 1.4\ \mu m^2$. Before manufacturing we remove the microlens layer and the colour filter. Further information on the pretreatments and fabrication can be found in the Methods. In Fig. 5b an SEM image of a hexagonal arrangement of 19 printed doublet lenses is shown. Each individual lens shows uniformly high quality and performs very similarly to neighbouring lenses. Image acquisitions confirm the optical quality. Figure 5c depicts the image of a part of the USAF 1951 resolution test chart taken through a hexagonal multi-element lens arrangement. The image part has a size of 640 × 480 pixels, and the chart is at a distance of 30 mm. The numbers and lines of the elements of group −2 can be clearly distinguished. Each lens has a diameter of 120 μm and an imaging area with a diameter of around 100 μm. This area contains about 4,000 pixels. Each doublet lens creates images with the same performance as its neighbour. This corroborates the fact that femtosecond direct laser writing is extremely well suited for the reliable and reproducible fabrication of multiple identical or different 3D printed compound micro-optics, even on large sensor areas. Thus, high quality and high acceptance angle Shack–Hartmann wavefront sensors consisting of a regular arrangement of multi-lens systems can also be fabricated (see Supplementary Fig. 3, which displays a similar lens array, but with triplet lens elements).

An endoscopic application on the micrometre scale can be realized by using an imaging fibre with a total outer diameter of only 210 μm. We manufactured a triplet objective lens (the same as the one in Fig. 2) with five refractive interfaces directly on the end facet of the fibre. Figure 6a depicts a microscope side view of the micro-optical lens system. For the writing process the triplet lens is centred by illuminating the opposite end facet and aligning it with respect to the writing beam. The Materials and Methods section in the Supplementary Information contains more details on the fabrication process. Figure 6b depicts the set-up that is used for the measurement of the optical performance. The opposite fibre end facet is then imaged using an optical microscope with 50× objective with a numerical aperture (NA) of 0.55. The active area of the fibre has a diameter of 145 μm, whereas the 3D printed objective provides an imaging area with a diameter of 100 μm. Therefore, the active area contains roughly 700 of the 1.600 pixels. As each pixel has a pixel diameter of 4 μm the resolution is limited by this specific

fibre geometry. Figure 6c displays the images of a small section of the USAF 1951 resolution test chart. The image is transfered through a 170 cm long fibre piece. The notifications of the elements 3 to 6 of group 0 are clearly recognizable. As an example the number 6 (bottom right) of group 0 has a height of about 1.6 mm. The test target is mounted at a distance of 3 mm from the fiber end facet, resembling typical endoscopic situations in medical imaging.

Conclusion and outlook

We have demonstrated the femtosecond direct laser writing of various ultracompact compound lens systems with numerous refractive surfaces. The lenses show unprecedented performances and high optical quality with resolutions of up to 500 lp mm^{-1} for imaging applications. This method gives submicrometre accuracy and extremely good reproducibility, allowing for fast and reliable transfer from design and simulations to high-performance printed optics. Our approach creates a completely new platform for the fabrication of optical multi-lens systems for high-quality imaging on the micrometre scale with a plethora of applications in numerous fields that were previously unavailable. We have proven that the capabilities of additive manufacturing can be used for the fabrication of high-quality micro- and nano-optical elements and objective lenses. In the future, optical hybrid systems consisting of a combination of refractive, diffractive and reflective elements can be easily manufactured by femtosecond direct laser writing. Consequently, our method allows for complex free-form optics with numerous surfaces and features that show high optical performance and tremendous compactness, with sizes at least one order of magnitude smaller than current approaches. Our optical elements thus allow for a completely new generation of ultracompact optical elements for endoscopic instruments and miniaturized microscopes to be used in medical engineering—for live neuro-imaging in the brain, for example. High-NA trapping with optical fibres, optical elements on the wafer level (such as high-quality imaging directly on CMOS sensors for miniaturized robots and drones) or quantum emitters (for example, nitrogen–vacancy centres in diamond or quantum dots that are combined with their own high-NA collection and imaging optics) are possible.

Combining different optical materials for 3D printing may compensate chromatic and spherical aberrations in an achromatic lens design. Alternatively, the achromatic correction can be achieved by the combination of refractive and diffractive surfaces. An extra antireflection coating generated by ALD, moth-eye based structures[26] or other surface treatments will further enhance the optical performance. Anti-reflection coatings would reduce stray light and improve the image contrast and efficiency. Optimization of the contour accuracy will further improve the performance. For example, jet printing[27] of thin polymer layers on top of our lenses might reduce the surface roughness further. Fabrication errors can be reduced by minimizing the shrinkage of the photoresists during the fabrication process by using suitable polymers. Alternatively, the adaption of the shape of the compound lens elements can compensate the shrinking of the materials during development. Using pressure[28], fluids[29–31] in microchannels or active materials such as switchable metasurfaces[32–34], static multi-lens systems can be converted into flexible zoom lenses and hence adjustable foci could become a possibility. Inked photosensitive materials, or the subsequent and specific filling of cavities, will allow for the fabrication of apertures that further improve the optical performance. Catadioptric system designs have the advantage of reducing chromatic aberrations and thereby reducing the size of the optical system even more.

Micro-optical systems containing one or more free-form surfaces are now available. Complex elements for beam shaping, endoscopy, illumination, high-performance imaging, inspection and microscopy on the micrometre scale are thus possible. Multi-element optical systems and even imaging systems with dimensions on the order of a grain of salt can be realized. This will lead to a plethora of novel devices with tremendous impact on biotechnology, medical engineering and safety/security monitoring.

Methods

Methods and any associated references are available in the online version of the paper.

Received 17 January 2016; accepted 13 May 2016; published online 27 June 2016

References

1. Vaezi, M., Seitz, H. & Yang, S. A review on 3D micro-additive manufacturing technologies. *Int. J. Adv. Manuf. Technol.* **67,** 1721–1754 (2013).
2. Popovic, Z. D., Sprague, R. A. & Connell, G. A. N. Technique for monolithic fabrication of microlens arrays. *Appl. Opt.* **27,** 1281–1284 (1988).
3. Lee, S.-K., Lee, K.-C. & Lee, S. S. A simple method for microlens fabrication by the modified LIGA process. *J. Micromech. Microeng.* **12,** 334–340 (2002).
4. Lee, B.-K., Kim, D. S. & Kwon, T. H. Replication of microlens arrays by injection molding. *Microsyst. Technol.* **10,** 531–535 (2004).
5. Kim, J. Y. *et al.* Hybrid polymer microlens arrays with high numerical apertures fabricated using simple ink-jet printing technique. *Opt. Mater. Express* **1,** 259–269 (2011).
6. Völkel, R., Eisner, M. & Weible, K. J. Miniaturized imaging systems. *Microelectron. Eng.* **67–68,** 461–472 (2003).
7. Kuang, D., Zhang, X., Gui, M. & Fang, Z. Hexagonal microlens array fabricated by direct laser writing and inductively coupled plasma etching on organic light emitting devices to enhance the outcoupling efficiency. *Appl. Opt.* **48,** 974–978 (2009).
8. Yang, R., Wang, W. & Soper, S. A. Out-of-plane microlens array fabricated using ultraviolet lithography. *Appl. Phys. Lett.* **86,** 1–3 (2005).
9. Völkel, R. *et al.* Technology trends of microlens imprint lithography and wafer level cameras (WL). In *MOC'08, Conference on Micro-Optics*. Brussels, Belgium, 25–27 September (Microoptics Group, 2008).
10. Hoy, C. L. *et al.* Miniaturized probe for femtosecond laser microsurgery and two-photon imaging. *Opt. Express* **16,** 9996–10005 (2008).
11. Biehl, S., Danzebrink, R., Oliveira, P. & Aegerter, M. A. Refractive microlens fabrication by ink-jet process. *J. Sol-Gel Sci. Technol.* **13,** 177–182 (1998).
12. Brückner, A. *et al.* Ultra-thin wafer-level camera with 720p resolution using micro-optics. In *Proc. SPIE: Novel Optical Systems Design and Optimization XVII 91930W* (eds Gregory, G. G. & Davis, A. J.) (SPIE, 2014).
13. Cumpston, B. H. *et al.* Two-photon polymerization initiators for three-dimensional optical data storage and microfabrication. *Nature* **398,** 51–54 (1999).
14. Deubel, M. *et al.* Direct laser writing of three-dimensional photonic-crystal templates for telecommunications. *Nature Mater.* **3,** 444–447 (2004).
15. Farsari, M. & Chichkov, B. N. Materials processing: two-photon fabrication. *Nature Photon.* **3,** 450–452 (2009).
16. Sinzinger, S. & Jahns, J. *Microoptics* (Wiley Verlag GmbH & Co. KGaA, 2003).
17. Zappe, H. *Fundamentals of Micro-Optics* (Cambridge Univ. Press, 2010).
18. Malinauskas, M. *et al.* A femtosecond laser-induced two-photon photopolymerization technique for structuring microlenses. *J. Opt.* **12,** 035204 (2010).
19. Malinauskas, M. *et al.* Femtosecond laser polymerization of hybrid/integrated micro-optical elements and their characterization. *J. Opt.* **12,** 124010 (2010).
20. Williams, H. E., Freppon, D. J., Kuebler, S. M., Rumpf, R. C. & Melino, M. A. Fabrication of three-dimensional micro-photonic structures on the tip of optical fibers using SU-8. *Opt. Express* **19,** 22910–22922 (2011).
21. Malinauskas, M., Farsari, M., Piskarskas, A. & Juodkazis, S. Ultrafast laser nanostructuring of photopolymers: a decade of advances. *Phys. Rep.* **533,** 1–31 (2013).
22. Gissibl, T., Schmid, M. & Giessen, H. Spatial beam intensity shaping using phase masks on single-mode optical fibers fabricated by femtosecond direct laser writing. *Optica* **3,** 448–451 (2016).
23. Han, H., Kriman, M. & Boomgarden, M. Wafer level camera technology - from wafer level packaging to wafer level integration. In *11th International Conference on Electronic Packaging Technology and High Density Packaging* (IEEE, 2010).
24. Bückmann, T. *et al.* Tailored 3D mechanical metamaterials made by dip-in direct-laser-writing optical lithography. *Adv. Mater.* **24,** 2710–2714 (2012).
25. Dunkel, J. *et al.* Fabrication of refractive freeform array masters for artificial compound eye cameras. *Proc. SPIE: Micro-Optics* **9130,** 91300P (2014).
26. Kowalczyk, M., Haberko, J. & Wasylczyk, P. Microstructured gradient-index antireflective coating fabricated on a fiber tip with direct laser writing. *Opt. Express* **22,** 12545–12550 (2014).
27. Blattmann, M., Ocker, M., Zappe, H. & Seifert, A. Jet printing of convex and concave polymer micro-lenses. *Opt. Express* **23,** 24525–24536 (2015).

28. Zhang, W., Aljasem, K., Zappe, H. & Seifert, A. Highly flexible MTF measurement system for tunable micro lenses. *Opt. Express* **18,** 12458–12469 (2010).
29. Werber, A. & Zappe, H. Tunable microfluidic microlenses. *Appl. Opt.* **44,** 3238–3245 (2005).
30. Friese, C., Werber, A., Krogmann, F., Mönch, W. & Zappe, H. Materials, effects and components for tunable micro-optics. *IEEJ Trans. Electr. Electron. Eng.* **2,** 232–248 (2007).
31. Song, C., Nguyen, N.-T., Tan, S.-H. & Asundi, A. K. Modelling and optimization of micro optofluidic lenses. *Lab Chip* **9,** 1178–1184 (2009).
32. Michel, A. K. U. *et al.* Using low-loss phase-change materials for mid-infrared antenna resonance tuning. *Nano Lett.* **13,** 3470–3475 (2013).
33. Yu, N. & Capasso, F. Flat optics with designer metasurfaces. *Nature Mater.* **13,** 139–150 (2014).
34. Yin, X. *et al.* Active chiral plasmonics. *Nano Lett.* **15,** 4255–4260 (2015).

Acknowledgements

We gratefully acknowledge financial support from the DFG (SPP1391, FOR730 and GI 269/11-1), BMBF (13N10146, PRINTOPTICS), Baden-Württemberg Stiftung (Internationale Spitzenforschung II and Intelligente Optische Sensorik) and ERC (COMPLEXPLAS). We would like to thank B. Frank for performing atomic force microscope measurements and T. Mappes from Carl Zeiss AG for help with the lens characterization. We would like to thank M. Grauer for strong support.

Author contributions

T.G., S.T. and H.G. conceived the concept. T.G. performed simulations, structural designs, direct laser writing and experimental characterization. S.T. and A.H. were responsible for optical and structural design. H.G. participated in planning the experiments and supervised the project. All authors participated in discussions and contributed to writing of the manuscript.

Additional information

Supplementary information is available in the online version of the paper. Reprints and permissions information is available online at www.nature.com/reprints. Correspondence and requests for materials should be addressed to T.G.

Competing financial interests

The authors declare no competing financial interests.

Methods

Simulation. The compound lenses are designed and optimized within the optical design software ZEMAX using a combination of ray- and wave-optical approaches. We used 1.513 as the refractive index of the lens material. The refractive index value is confirmed by measuring the critical total internal reflection angle of the photoresist at different wavelengths. An even aspheric surface parameterization is used as the surface type of the refractive interfaces. The lens diameters are around 120 μm and the thicknesses of the compound lenses vary between 120 and 200 μm. The active optical areas for imaging have a diameter of 100 μm. The lens designs are exported into a computer-aided design file format and afterwards transformed into a stereolithographic file format. The simulation results of Figs 2b and 3d are also achieved by using the optical design software ZEMAX.

Sample fabrication. The compound lenses are fabricated by direct laser writing using a commercially available femtosecond laser lithography system (Nanoscribe Photonic Professional GT)[14,15]. The numerous compound lenses are exposed by two-photon absorption in an ultraviolet sensitive photoresist (IP-S, Nanoscribe GmbH, Germany) at a wavelength of 780 nm. A dip-in lithography configuration is used to fabricate these bulky structures[24]. The designed structures are written layer-by-layer with a distance of 100 nm between the individual layers. For this, ultraprecise piezo actuators move the sample in the axial direction after fabricating each layer. In the lateral direction the laser beam is guided by galvanometric mirrors parallel to the substrate. After the writing process, the lenses are developed in a bath of developer (mr-dev 600 for IP-photoresist) for 20 min and a subsequent rinsing bath of isopropanol for 2 min. The fabrication method allows for optical elements with an unprecedented high optical quality.

Dip-in laser lithography is not limited to specific substrates, small optical element volumes or particular fabrication heights. We demonstrate imaging with compound lenses manufactured on glass substrates (Figs 1–4 and Supplementary Figs 1–3), on CMOS sensors (Fig. 5) and on the end facets of imaging fibres (Fig. 6).

As an image sensor we use an Omnivision 5647 CMOS image sensor from a Raspberry Pi Camera Module. The sensor has a pixel size of $1.4 \times 1.4\ \mu m^2$. Before manufacture on the sensor, we scrape off the microlens layer using a wooden spatula. We use FTIFHR160S-1600 (F&T Fibers and Technology GmbH, Berlin, Germany) as the image fibres. The fibre has 1,600 single mode cores, where each one acts a single pixel. The active image area has a diameter of 145 μm and therefore each pixel has a diameter of about 4 μm. The fibre is mounted using a standard fibre holder with a V-shaped groove (Elliot Martock MDE 710) directly attached to the lithography system. The compound lenses can be centred by illuminating the opposite end of the fibre and observing the end facet with a CCD camera. The fibre can be perfectly aligned with respect to the writing beam by using the ultraprecise piezo actuators of the laser lithography system. The fabrication method allows for the fabrication of imaging fibres with undefined fibre lengths. In our case, the fibre has a length of 170 cm. The image fibre is directly cleaved before the writing process by a standard fibre cleaver.

Measurement. The performance of the compound lenses is analysed by imaging the projection on the last surface by microscope objectives (Nikon CFI LU Plan Fluor BD 10×, Nikon CFI LU Plan Fluor BD 20×, Nikon CFI LU Plan BD ELWD 50× and Nikon CFI LU Plan BD ELWD 100×) onto a CCD camera (GC 2450C, Allied Vision Technologies). We use an industrial upright microscope (Nikon Eclipse LV100-DA). The test charts are illuminated using the light source for diascopic illumination in combination with a condenser (Nikon LWD achromat condenser NA 0.65).

The MTF in Fig. 3 is measured by using the knife-edge method. The sharp edge of a razor blade is imaged by the compound lens and a 50× objective (Nikon CFI LU Plan BD ELWD 50×) onto the CCD sensor at various positions and at different orientations. The images are analysed by summing up the edge spread function over a certain image region indicated by the small arrows in Supplementary Fig. 2. The averaged edge spread function is differentiated to obtain the line spread function, which is again Fourier transformed to obtain the MTF presented in Fig. 3.

The longitudinal (axial) chromatic aberrations are measured by using 40 nm bandwidth optical filters at different wavelengths. At each wavelength, the focal shift is determined by adjusting the axial position of the compound lens.

To analyse the performance of the CMOS sensor the image is read out using the Raspberry Pi command raspistill. The quality of the triplet lens fabricated on the end facet of an image fibre is analysed by observing the opposite end of the fibre with a microscope objective.

The images are modified by enhancing the contrast and adjusting the brightness, except for the images that are used for the calculation of the MTF. Some images are converted from a true-colour image to a greyscale intensity image to remove the colour cast.